Bifurcation of Switched Nonlinear Dynamical Systems

Takuji Kousaka, *Member, IEEE,* Tetsushi Ueta, *Member, IEEE,* and Hiroshi Kawakami, *Member, IEEE*

***Abstract*—This paper proposes a method to trace bifurcation sets for a piecewise-defined differential equation. In this system, the trajectory is continuous, but it is not differentiable at break points of the characteristics. We define the Poincaré mapping by suitable local sections and local mappings, and thereby it is possible to calculate bifurcation parameter values. As an illustrated example, we analyze the behavior of a two-dimensional nonlinear autonomous system whose state space is constrained on two half planes concerned with state-dependent switching characteristics. From investigation of bifurcation diagrams, we conclude that the tangent and global bifurcations play an important role for generating various periodic solutions and chaos. Some theoretical results are confirmed by laboratory experiments.**

***Index Terms*—Bifurcation, piecewise-defined differential equation, Poincaré mapping.**

I. Introduction

AN ELECTRIC circuit containing a switch controlled by various conditions can exhibit many interesting phenomena. The differential equations, including discontinuous characteristics derived from such switched systems, have been studied for a long time since their dynamical systems are easily realized by comparators, relays, switches, diodes, and so on.

Many systems described by piecewise-linear differential equations have been investigated [1]–[5]. These chaotic circuits contained a negative resistance, a hysteresis element, an ideal diode, etc. In these cases, obtaining bifurcation parameter values and evidence of chaos are directly derived by analytical method, because the system can be solved exactly.

On the other hand, in a case where the system is described by nonlinear differential equation, it is impossible to calculate the exact solution. Besides, there is no investigation of the system described by a differential equation with piecewise-nonlinear functions.

In this paper, we consider the system with nonsmooth and nonlinear characteristics, i.e., piecewise-nonlinear system, and investigate bifurcation problems in this system. First, we define a piecewise-defined system, its solution, and limit cycle. Then we propose a method to calculate bifurcation parameter values for this systems. Local sections are naturally defined at the break points, and the Poincaré mapping is constructed as a composite map of local mappings. The parameter values of local bifurcations and the location of the fixed point are calculated by Newton's method using these mappings. Second, we focus on a concrete circuit example. This example mainly contains three bifurcation phenomena: tangent, period-doubling, and global bifurcations. After the global bifurcation, a limit cycle disappears since the orbit touches the boundary (threshold value) tangentially. This is a singular property of the system with the state-dependent switch. We can calculate bifurcation parameter values where the bifurcation occurs. We also grasp the whole structure of bifurcation sets in the parameter space. From investigation of bifurcation diagrams, we conclude that the tangent and the global bifurcations play an important role for generating various periodic solutions and chaos of this system. The theoretical results have been verified in laboratory experiments. Our method is not for a specific system; consequently, it can be applied to general piecewise-linear and nonlinear systems, e.g., boost converters [6], [7], biological systems [8], [9], etc.

Manuscript received October 18, 1998; revised March 9, 1999. This paper was recommended by Guest Editors F. Maloberti and R. Newcomb.

T. Kousaka and T. Ueta are with the Department of Information Science and Intelligent Systems, Tokushima University, Tokushima, 770-8506 Japan.

H. Kawakami is with the Department of Electrical and Electronic Engineering, Tokushima University, Tokushima, 770-8506 Japan.

Publisher Item Identifier S 1057-7130(99)05642-6.

II. Analyzing Method of Piecewise-Defined Differential Equation

Let us consider m autonomous differential equations

$$\frac{d\boldsymbol{x}}{dt} = \boldsymbol{f}_k(\boldsymbol{x}, \lambda, \boldsymbol{\lambda}_k), \qquad k = 0, 1, 2, \cdots, m-1 \tag{1}$$

where $t \in \boldsymbol{R}, \boldsymbol{x} \in \boldsymbol{R}^n$. $\boldsymbol{\lambda} \in \boldsymbol{R}^r$ is an invariant parameter for $\boldsymbol{f}_0$, $\boldsymbol{f}_1, \cdots, \boldsymbol{f}_{m-1}$ and $\boldsymbol{\lambda}_k \in \boldsymbol{R}^s$ is a parameter depending only on $\boldsymbol{f}_k$. r and s are integers. We call these equations *piecewise-defined differential equations*. Assume that $\boldsymbol{f}_k$ is C^∞-class map for all variables and parameters and every equation in (1) has a solution with an arbitrary initial value $\boldsymbol{x}_{i0}$, such that

$$\boldsymbol{x}_k(t) = \boldsymbol{\varphi}_k(t, \boldsymbol{x}_{i0}), \quad \boldsymbol{x}_k(0) = \boldsymbol{x}_{k0}. \tag{2}$$

Assume also that the function changes from $\boldsymbol{f}_k$ to $\boldsymbol{f}_{k+1}$ when a solution $\boldsymbol{\varphi}_k$ starting from Π_k reaches Π_{k+1} with time τ_k. Each solution of (1) is written as

$$\boldsymbol{x}_{k+1}(t) = \boldsymbol{\varphi}_i(t, \boldsymbol{x}_i) \tag{3}$$

where

$$\boldsymbol{x}_{i+1} = \boldsymbol{\varphi}_{k+1}(0, \boldsymbol{x}_{k+1}) = \boldsymbol{\varphi}_k(\tau_k, \boldsymbol{x}_k). \tag{4}$$

A periodic solution (limit cycle) is written as

$$\boldsymbol{x}_0 = \boldsymbol{x}_m = \boldsymbol{\varphi}_{m-1}(\tau_{m-1}, \boldsymbol{x}_{m-1}). \tag{5}$$

Note that the solution (3) is continuous, but not differentiable for all states. We place local section for this limit cycle at every break point defined by the following scalar function q_i:

$$\Pi_k = \{\boldsymbol{x}_k \in \boldsymbol{R}^n | q_k(\boldsymbol{x}_k) = 0\}, \qquad k = 0, 1, 2, \cdots, m-1. \tag{6}$$

The following local mappings are defined (see Fig. 1):

$$\begin{aligned} T_0\colon\ & \Pi_0 \to \Pi_1 \\ & \boldsymbol{x}_0 \mapsto \boldsymbol{x}_1 = \boldsymbol{\varphi}_0(\tau_0, \boldsymbol{x}_0) \\ T_1\colon\ & \Pi_1 \to \Pi_2 \\ & \boldsymbol{x}_1 \mapsto \boldsymbol{x}_2 = \boldsymbol{\varphi}_1(\tau_1, \boldsymbol{x}_1) \\ & \cdots \\ T_{m-1}\colon\ & \Pi_{m-1} \to \Pi_0 \\ & \boldsymbol{x}_{m-1} \mapsto \boldsymbol{x}_0 = \boldsymbol{\varphi}_{m-1}(\tau_{m-1}, \boldsymbol{x}_{m-1}). \end{aligned} \tag{7}$$

Poincaré mapping is defined as a differentiable mapping described by

$$T = T_0 \circ T_1 \circ \cdots \circ T_{m-1}. \tag{8}$$

Hence, the period of the limit cycle τ is obtained by

$$\tau = \sum_{k=0}^{m-1} \tau_k. \tag{9}$$

The derivative with the initial value of the Poincaré map is given by

$$\left.\frac{\partial T}{\partial \boldsymbol{x}_0}\right|_{t=\tau} = \prod_{k=0}^{m-1} \left.\frac{\partial T_k}{\partial \boldsymbol{x}_k}\right|_{t=\tau_k}. \tag{10}$$

Each Jacobian matrix can be written as follows:

$$\frac{\partial T_k}{\partial \boldsymbol{x}_k} = \frac{\partial \boldsymbol{\varphi}_k}{\partial \boldsymbol{x}_k} + \frac{\partial \boldsymbol{\varphi}_k}{\partial t}\frac{\partial \tau_k}{\partial \boldsymbol{x}_k} = \frac{\partial \boldsymbol{\varphi}_k}{\partial \boldsymbol{x}_k} + \boldsymbol{f}_k \frac{\partial \tau_k}{\partial \boldsymbol{x}_k}. \tag{11}$$

We should remark that the function

$$q_k(\boldsymbol{x}_k) = q_k(\boldsymbol{\varphi}_k(\tau_k, \boldsymbol{x}_k)) = 0 \tag{12}$$

is differentiable for $\boldsymbol{x}_k$. Thereby

$$\frac{\partial q_k}{\partial \boldsymbol{x}_k}\left(\frac{\partial \boldsymbol{\varphi}_k}{\partial \boldsymbol{x}_k} + \boldsymbol{f}_k \frac{\partial \tau_k}{\partial \boldsymbol{x}_k}\right) = \boldsymbol{0} \tag{13}$$

where $q_m = q_0$. Assume that the orbit is transversal to all sections

$$\frac{\partial q_k}{\partial \boldsymbol{x}} \cdot \boldsymbol{f}_k \neq 0 \tag{14}$$

then we have the following relationship from (13):

$$\frac{\partial \tau_k}{\partial \boldsymbol{x}_k} = -\frac{1}{\dfrac{\partial q_k}{\partial \boldsymbol{x}}\boldsymbol{f}_k}\frac{\partial q_k}{\partial \boldsymbol{x}}\frac{\partial \boldsymbol{\varphi}_k}{\partial \boldsymbol{x}_k}. \tag{15}$$

By substituting (15) into (11), we have

$$\begin{aligned} \frac{\partial T_k}{\partial \boldsymbol{x}_k} &= \frac{\partial \boldsymbol{\varphi}_k}{\partial \boldsymbol{x}_k} - \frac{1}{\dfrac{\partial q_k}{\partial \boldsymbol{x}}\boldsymbol{f}_k}\boldsymbol{f}_k \frac{\partial q_k}{\partial \boldsymbol{x}}\frac{\partial \boldsymbol{\varphi}_k}{\partial \boldsymbol{x}_k} \\ &= \left[\boldsymbol{I}_n - \frac{1}{\dfrac{\partial q_k}{\partial \boldsymbol{x}} \cdot \boldsymbol{f}_k}\boldsymbol{f}_k \frac{\partial q_k}{\partial \boldsymbol{x}}\right]\frac{\partial \boldsymbol{\varphi}_k}{\partial \boldsymbol{x}_k} \end{aligned} \tag{16}$$

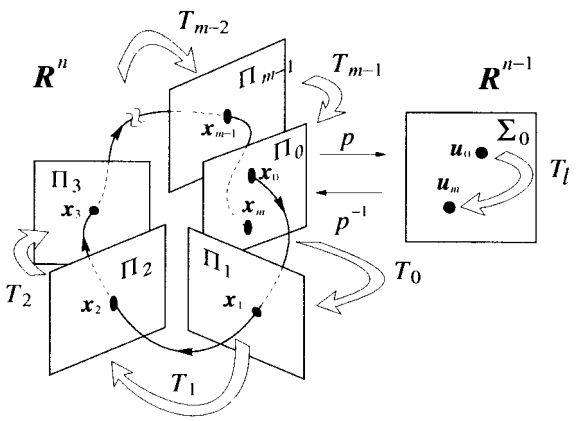

Fig. 1. Local sections and a trajectory.

where $\boldsymbol{I}_n$ is an $n \times n$ identity matrix. $\partial \boldsymbol{\varphi}_k / \partial \boldsymbol{x}_k$ can be obtained by solving the following differential equation:

$$\begin{aligned} &\frac{d}{dt}\left(\frac{\partial \boldsymbol{\varphi}_k}{\partial \boldsymbol{x}_k}\right) = \frac{\partial \boldsymbol{f}_k}{\partial \boldsymbol{x}}\left(\frac{\partial \boldsymbol{\varphi}_k}{\partial \boldsymbol{x}_k}\right) \\ &\left.\frac{\partial \boldsymbol{\varphi}_k}{\partial \boldsymbol{x}_k}\right|_{t=0} = \boldsymbol{I}_n, \qquad k = 0, 1, 2, \cdots, m-1. \end{aligned} \tag{17}$$

Now we define a local coordinate $\boldsymbol{u} \in \Sigma_0 \subset \boldsymbol{R}^{n-1}$ corresponding to Π_0 by using a projection p and embedding map p^{-1}

$$p^{-1}\colon \Sigma_0 \to \Pi_0, \quad p\colon \Pi_0 \to \Sigma_0. \tag{18}$$

Accordingly, the Poincaré mapping on the local coordinate is obtained as

$$\begin{aligned} T_\ell\colon\ & \Sigma_0 \to \Sigma_0 \\ & \boldsymbol{u} \mapsto p \circ T \circ p^{-1}(\boldsymbol{u}). \end{aligned} \tag{19}$$

A fixed point of the Poincaré mapping is obtained by solving the following equation:

$$T_\ell(\boldsymbol{u}) - \boldsymbol{u} = \boldsymbol{0}. \tag{20}$$

The Jacobian matrix which is needed in Newton's method is given by

$$\frac{\partial T_\ell}{\partial \boldsymbol{u}_0} = DT_\ell(\boldsymbol{u}_0) = \frac{\partial p}{\partial \boldsymbol{x}}\frac{\partial T}{\partial \boldsymbol{x}_0}\frac{\partial p^{-1}}{\partial \boldsymbol{u}}. \tag{21}$$

The characteristic equation for the fixed point is given by

$$\chi_\ell(\mu) = |DT_\ell - \mu \boldsymbol{I}_{n-1}| = 0. \tag{22}$$

The roots of (22) $\mu_1, \mu_2, \cdots, \mu_{n-1}$ give multipliers of the fixed points. We can obtain accurate location of the fixed point $\boldsymbol{u}$ and bifurcation parameter value λ by solving the following equation by Newton's method:

$$F(\boldsymbol{u}, \lambda) = \begin{bmatrix} T_\ell(\boldsymbol{u}) - \boldsymbol{u} \\ \chi_\ell(\mu) \end{bmatrix} = \boldsymbol{0}. \tag{23}$$

Now we should emphasize that to take the projection and embedding maps is indispensable to analyze the piecewise-defined nonlinear system. In the system whose states and parameters are smooth for all conditions, the multiple-shooting algorithm [10] is available, and the following characteristic

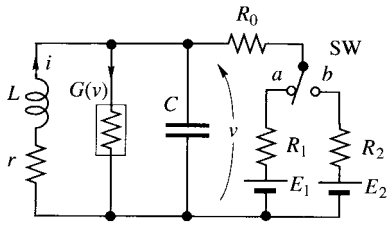

Fig. 2. The Alpazur oscillator.

equation of degree n is investigated for stability analysis of the fixed point:

$$\left| \prod_{k=0}^{m-1} \left. \frac{\partial \boldsymbol{\varphi}_k}{\partial \boldsymbol{x}_k} \right|_{t=\tau_k} - \mu \boldsymbol{I}_n \right| = 0. \tag{24}$$

However, in the system whose characteristics are discontinuous, correct multipliers are not obtained by solving (24). Correct $n-1$ multipliers, except for unity, are obtained by solving the characteristic equation (22) for all periodic orbits in any switched dynamical system. This means that taking the local coordinate Σ_i and considering bifurcation problems on these sections is essential for analysis of such discontinuous dynamical systems.

III. The Alpazur Oscillator

In this section, we consider a circuit model, called the Alpazur oscillator, proposed by Kawakami and Lozi [4], shown in Fig. 2. It has a switch and a nonlinear conductor. In [4], they analyzed a simple linear switched-dynamical system. In [2], a similar piecewise-linear hysteresis circuit has been proposed. They derived the one-dimensional return map rigorously by using exact solution of the circuit equation. From the return map, a sufficient condition for chaos generation and two parameter bifurcation diagram were given.

In the following, we use a nonlinear conductor instead of the linear one. This model should then be treated as a piecewise-defined system, and cannot be analyzed in a rigorous way any longer; only numerical methods, such as those stated in Section II, are available for bifurcation problems in this system. We derive a normalized equation from the circuit equation, and obtain bifurcation diagrams. Experimental results are also shown as confirmation.

A. Normalized Equation and the Poincaré Mapping

In Fig. 2, we assume that the nonlinear characteristic of the conductor G is the smooth cubic function, such that

$$G(v) = -a_1 v + a_3 v^3 \tag{25}$$

and, by using suitable transformation and rescaling for variables, the dynamical system of the circuit is described by piecewise-defined differential equations.

If SW is turned toward a

$$\begin{aligned} \frac{dx}{dt} &= -kx - y = f_0 \\ \frac{dy}{dt} &= x + (1-g_1)y - \frac{1}{3}y^3 + B_1 = g_0 \end{aligned} \tag{26}$$

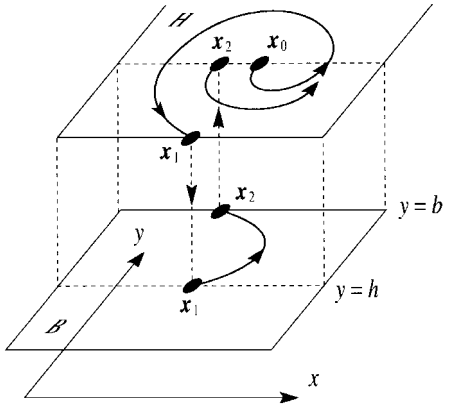

Fig. 3. Example of the trajectory of the Alpazur oscillator.

while, if SW is turned toward b, we have

$$\begin{aligned} \frac{dx}{dt} &= -kx - y = f_1 \\ \frac{dy}{dt} &= x + (1-g_2)y - \frac{1}{3}y^3 + B_2 = g_1. \end{aligned} \tag{27}$$

The orbit is trapped within two half planes and changed at their boundaries

$$\begin{aligned} H &= \{(x,y) \in \boldsymbol{R}^2 | y > h\} \\ B &= \{(x,y) \in \boldsymbol{R}^2 | y < b\} \\ \partial H &= \{(x,y) \in \boldsymbol{R}^2 | y = h\} \\ \partial B &= \{(x,y) \in \boldsymbol{R}^2 | y = b\}. \end{aligned} \tag{28}$$

Now we assume that $b > h$ (see Fig. 3). Behavior of the orbit is described as follows.

1) The flow starting from an arbitrary initial point moves within the half plane H or B, defined by (26) and (27), respectively.
2) If the flow reaches the edge ∂H or ∂B, then switching occurs; in other words, the switch is forced to act. Consequently, the flow jumps to the other half plane.

Since the characteristics of the switch have hysteresis, the flow generated by the mixed vector fields is complicated. Therefore, we expect many interesting phenomena in this model. Figs. 4 and 5 show stable orbits observed in the circuit with various values of B_1.

In the following, we briefly restate the method of analysis for this model. Let solutions on H and B be the following equations, respectively

$$\begin{aligned} x(t) &= \varphi_0(t, x_0, y_0, g_1, B_1, k) \\ y(t) &= \phi_0(t, x_0, y_0, g_1, B_1, k) \end{aligned} \tag{29}$$

$$\begin{aligned} x(t) &= \varphi_1(t, x_1, y_1, g_2, B_2, k) \\ y(t) &= \phi_1(t, x_1, y_1, g_2, B_2, k). \end{aligned} \tag{30}$$

Local sections and local mappings are defined as follows:

$$\begin{aligned} \Pi_0 &= \{\boldsymbol{u} \in B | q_0(x_1, y_1) = y - b = 0\} \\ \Pi_1 &= \{\boldsymbol{u} \in H | q_1(x_1, y_1) = y - h = 0\}. \end{aligned} \tag{31}$$

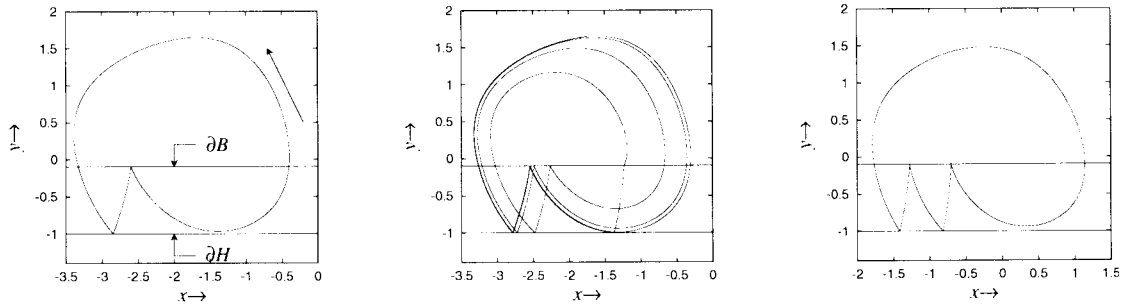

(a) (b) (c)

Fig. 4. Computer simulation-1. Stable orbits in the neighborhood of the global bifurcation curve $(B_2 = 5.0)$. (a) H_R^1 orbit $(B_1 = 1.86)$. (b) $H_R^4 H_S^1$ orbit $(B_1 = 1.785)$. (c) $H_R^1 H_S^1$ orbit $(B_1 = 0.145)$.

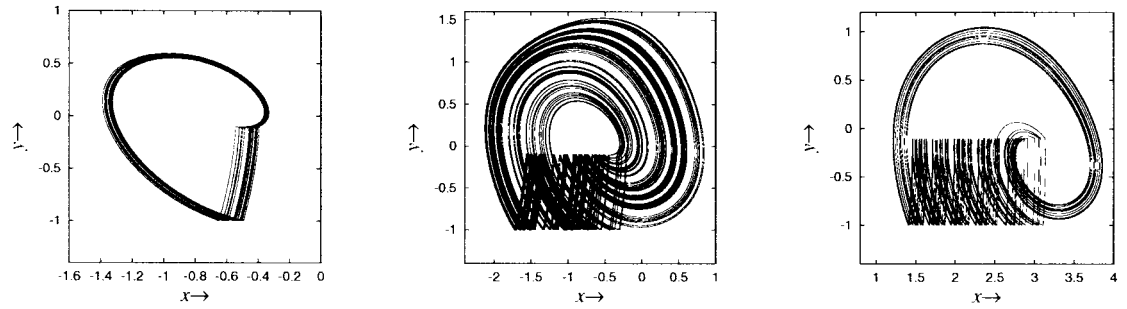

(a) (b) (c)

Fig. 5. Computer simulation-2. Chaotic attractor $(B_2 = 5.0)$. (a) $B_1 = 0.56$. (b) $B_1 = 0.5$. (c) $B_1 = -2.8$.

$$\begin{aligned} T_0\colon\ & \Pi_0 \to \Pi_1 \\ & x_0 \mapsto x_1 = \varphi_0(\tau_0, x_1, y_1, g_1, B_1, k) \\ & y_0 \mapsto y_1 = h \\ T_1\colon\ & \Pi_1 \to \Pi_0 \\ & x_1 \mapsto x_2 = \varphi_1(\tau_1, x_1, y_1, g_2, B_2, k) \\ & y_1 \mapsto y_2 = b. \end{aligned} \tag{32}$$

Thus, we have

$$T = T_0 \circ T_1. \tag{33}$$

We choose the projection and embedding as follows:

$$\begin{aligned} p\colon\ & \Pi_0 \to \Sigma_0, \qquad \boldsymbol{x} = \begin{bmatrix} x \\ y \end{bmatrix} \mapsto u = x \\ p^{-1}\colon\ & \Sigma_0 \to \Pi_0, \qquad u = x \mapsto \boldsymbol{x} = \begin{bmatrix} x \\ b \end{bmatrix}. \end{aligned} \tag{34}$$

The Jacobian matrix of the Poincaré mapping is as follows:

$$\begin{aligned} DT_\ell(\boldsymbol{u}) &= \frac{\partial p}{\partial \boldsymbol{x}} \frac{\partial T}{\partial \boldsymbol{x}_0} \frac{\partial p^{-1}}{\partial \boldsymbol{u}} \\ &= \left(\frac{\partial \varphi_0}{\partial x_0} - \frac{f_0}{g_0} \frac{\partial \phi_0}{\partial x_0} \right) \left(\frac{\partial \varphi_1}{\partial x_1} - \frac{f_1}{g_1} \frac{\partial \phi_1}{\partial x_1} \right). \end{aligned} \tag{35}$$

We can obtain the location of the fixed point $\boldsymbol{x}_0 = (x_0, b)$ and bifurcation parameter value by applying Newton's method to (23).

B. Periodic Orbit

In this paper, we fix the parameters for (26) and (27) as

$$k = 0.1, \quad g_1 = 0.2, \quad g_2 = 2.0, \quad h = -1.0, \quad b = -0.1. \tag{36}$$

Note that (26) has a stable limit cycle and (27) has a stable equilibrium point. By varying B_1 and B_2, the Alpazur oscillator exhibits interesting phenomena concerned with switching.

In order to define the period of a periodic orbit and classify its topological properties, we attach symbols to the orbit with respect to its shape in the phase portrait. A part of a periodic orbit moving within the half-plane H can be distinguished into two types.

1) H_S (sliding): a part of the periodic orbit starting from $y = b$ moves within H with $dy/dt \neq 0$ and switches at $y = h$.
2) H_R (rotating): a part of the periodic orbit starting from $y = b$ moves within H and has at least one $dy/dt = 0$ point and switches at $y = h$.

Any other parts followed after H_R or H_S must move within the half-plane B and switch at $y = b$. Then we classify a periodic orbit by using these symbols according to the order of appearance in the periodic orbit. The superscript $j = 1, 2, \cdots$ for H_S and H_R shows the number of their repetition in the periodic motion. The period is defend by the sum of the numbers of superscripts. For instance, the orbit of Fig. 4(c) is symbolized as $H_R^1 H_S^1$ and its period is 2. Note that (26) has a stable equilibrium point. Thus, it is required that the orbit

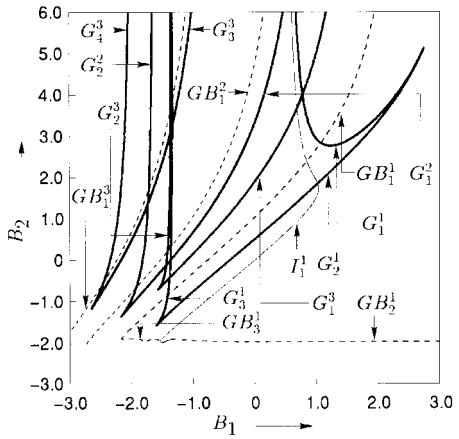

Fig. 6 Bifurcation diagram in B_1–B_2 plane.

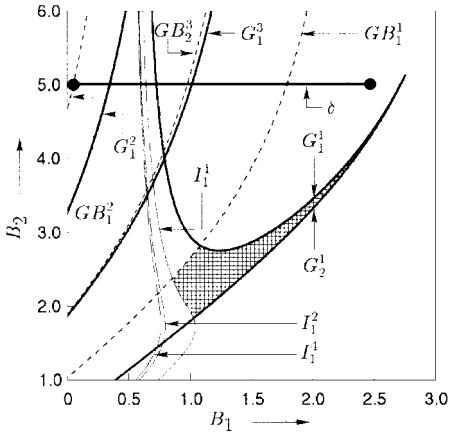

Fig. 8. Enlarged diagram-1 of Fig. 6.

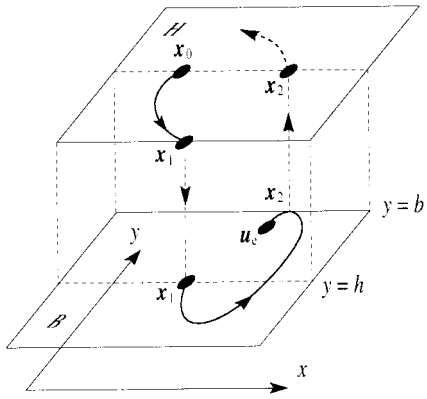

Fig. 7. Disappearance of H_R^1 orbit.

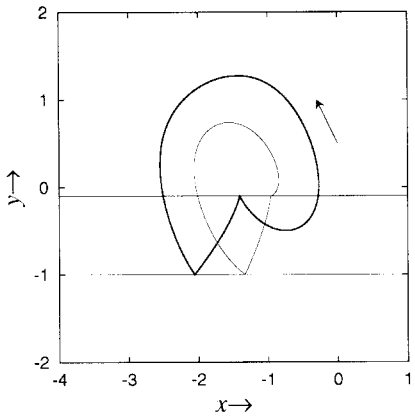

Fig. 9. Two stable H_R^1 orbits.

must reach $y = b$ transversally to form a periodic orbit. If not, the orbit will sink into the equilibrium.

C. Bifurcation Phenomena

We define symbols for bifurcation sets as follows: G_k^n and I_k^n are a tangent and period-doubling bifurcation set for n-periodic orbits, respectively, while GB_k^n is global bifurcation set for n-periodic orbits, where k is a nominal number.

Fig. 6 shows the bifurcation diagram of limit cycles for B_1–B_2 parameter plane. We only show the bifurcation sets until 3-periodic points. But another subharmonic bifurcation curves exist in these bifurcation diagrams. Typically, in the parameter regions surrounded by G^i (thick curves), there exist two stable periodic orbits and one saddle-type orbit. Each of them meets a local bifurcation or a global bifurcation individually as the parameter varies. For example, if the value of the parameter B_2 is smaller than GB_2^1 and GB_3^1, the global bifurcation occurs. Fig. 7 shows this phenomenon. If this model has a stable limit cycle, the orbit must reach $y = b$ transversally. If not, the orbits of the model settle into the stable equilibrium point $\boldsymbol{u}_e$, because the solution of B has a stable one.

Fig. 8 shows an enlargement of Fig. 6. In hatched area, we can observe two one-periodic stable periodic orbits, see Fig. 9. As the parameter B_1 decrease from this area, one of periodic orbits becomes unstable via period-doubling I_1^1, and a stable two-periodic orbit is generated. In the same way, the stable four-periodic orbits is generated by crossing I_1^2 bifurcation set. This bifurcation process shows the period doubling rout to chaos as the local bifurcation of this model. This type of chaotic attractor is shown in Fig. 5(a).

If the trajectory touches the boundary ∂B or ∂H tangentially, then global bifurcation occurs. For example, as parameter B_1 varies along δ in Fig. 8, another stable limit cycle of Fig. 9 meets GB_1^1. Then the limit cycle disappears and three-period orbit is generated [see Fig. 4(a) and (b)]. Thus, we can calculate this bifurcation by solving the following equation:

$$T_\ell^n(x_0) - x_0 = 0, \quad y|_{t=\tau_i} = 0, \quad \left.\frac{dy}{dt}\right|_{t=\tau_i} = 0. \tag{37}$$

This is a singular property of the system, including state-dependent switches, since these global bifurcations occur regardless of the stability of the Poincaré mapping for the periodic orbit. In general, we cannot anticipate what kind of orbit will be appeared after the global bifurcation.

Fig. 10 shows a one-parameter bifurcation diagram obtained by changing parameter B_1 along δ, $(B_2 = 5.0)$. We can see that some periodic orbits are collapsed by tangent bifurcation G_k^n and global bifurcation GB_k^n. There exist many period-doubling bifurcations for periodic orbits. In some values of B_1, a nonperiodic motion occurs [see Fig. 5(b) and (c)]. Fig. 11

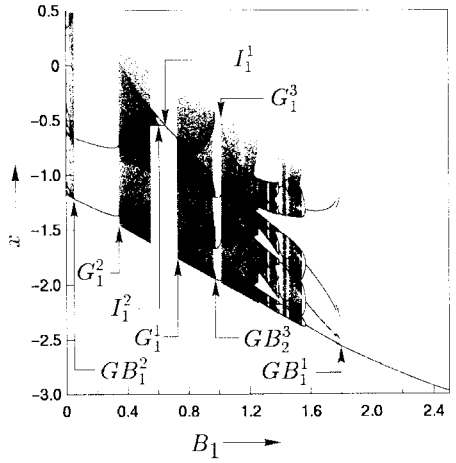

Fig. 10. One-parameter bifurcation diagram obtained along line δ in Fig. 8. $(B_2 = 5.0)$.

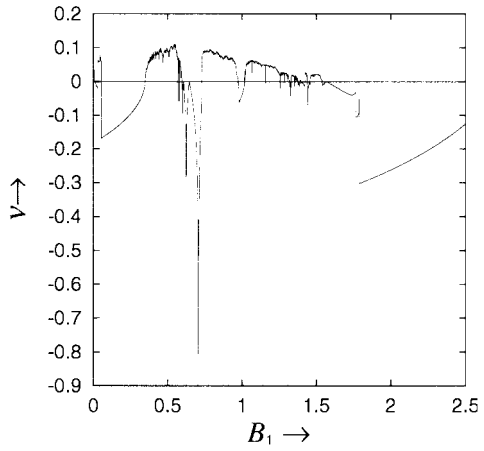

Fig. 11. Maximum Lyapunov exponent ν obtained along line δ in Fig. 8 $(B_2 = 5.0)$.

shows the corresponding maximum Lyapunov exponent for Fig. 10. The maximum Lyapunov exponent of these nonperiodic orbits indicates a positive value, so these orbits are considered to be chaos. Note that the maximum Lyapunov exponent can be calculated by solving the following equation:

$$\nu = \lim_{n\to\infty} \sum_{k=1}^{n} \frac{1}{t_k} \log ||DT_\ell^k|| \tag{38}$$

where $||\cdot||$ is an Euclidean norm and t_k indicates the return-time spending every cycle of the oscillation. In this case, calculation of the maximum Lyapunov exponent is comparatively easy because the derivative of the fixed points is a scalar value.

Fig. 12 shows an enlarged diagram of Fig. 6. It is noteworthy that the period-doubling set and some global bifurcation sets connect at a point, that is, a higher codimension bifurcation occur. The topological classification of periodic orbits near this point is complicated, since much switching occur within slightly different parameter values.

Fig. 13 is a one-parameter bifurcation diagram obtained along η in Fig. 12. The stable one-periodic orbit H_R^1 becomes unstable by crossing I_1^1, then the stable two-periodic orbit

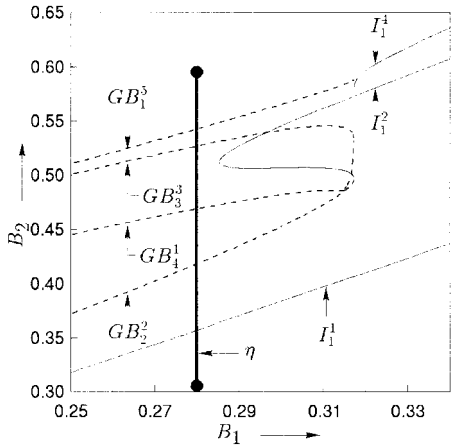

Fig. 12. Enlarged diagram-2 of Fig. 6.

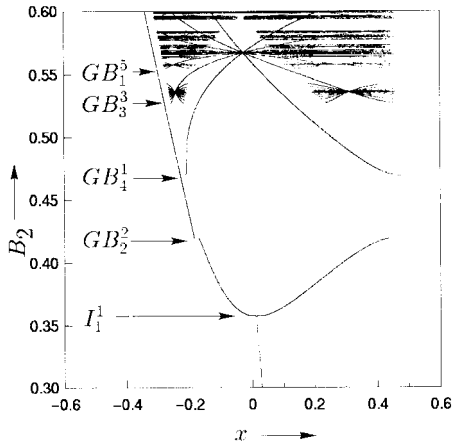

Fig. 13. One-parameter bifurcation diagram obtained along η in Fig. 12. $(B_1 = 0.28)$.

$(H_R^1)^2$ occurs, and if this orbit crosses GB_2^2 in the parameter plane, H_R^2 orbits appear. Moreover, this orbit crosses GB_4^1 and GB_3^3, the stable $H_R^2(H_R^1)^2$ orbits and $H_R^2(H_R^1)^6$ orbits occur, respectively. Although the global bifurcation is caused for a periodic orbit with parameter perturbation, the shape of the orbit is not changed dramatically, i.e., the orbit retains similar shape after the bifurcation.

D. Laboratory Experiments

We confirm the theoretical results of the Alpazur oscillator by laboratory experiments. The circuit equation of Fig. 2 is given as

$$\begin{cases} L\dfrac{di}{dt} = -v - ri \\ C\dfrac{dv}{dt} = i - G(v) + \dfrac{E_1 - v}{R_0 + R_1}, \end{cases} \quad \text{(if SW is at } a\text{)} \tag{39}$$

$$\begin{cases} L\dfrac{di}{dt} = -v - ri \\ C\dfrac{dv}{dt} = i - G(v) + \dfrac{E_2 - v}{R_0 + R_2}, \end{cases} \quad \text{(if SW is at } b\text{)}. \tag{40}$$

By rescaling

$$\hat{x} = \sqrt{L}i, \quad \hat{y} = \sqrt{C}v, \quad t' = \frac{1}{\sqrt{LC}}t \tag{41}$$

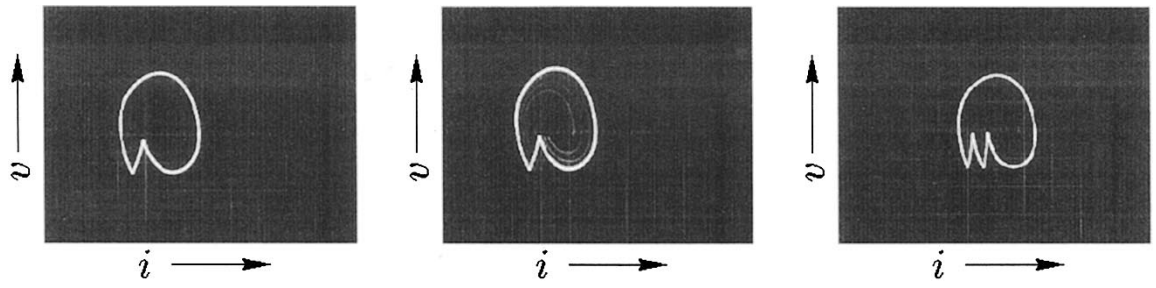

(a) (b) (c)

Fig. 14. Laboratory experiments-1. Stable orbits in the neighborhood of the global bifurcation curve ($E_2 = 5.19\,\mathrm{V}$). (a) H_R^1 orbit ($E_1 = 6.78\,\mathrm{V}$). (b) $H_R^4 H_S^1$ orbit ($E_1 = 6.63\,\mathrm{V}$). (c) $H_R^1 H_S^1$ orbit ($E_1 = 0.53\,\mathrm{V}$). (v: 2.0 V/div, i: 4.1 mA/div).

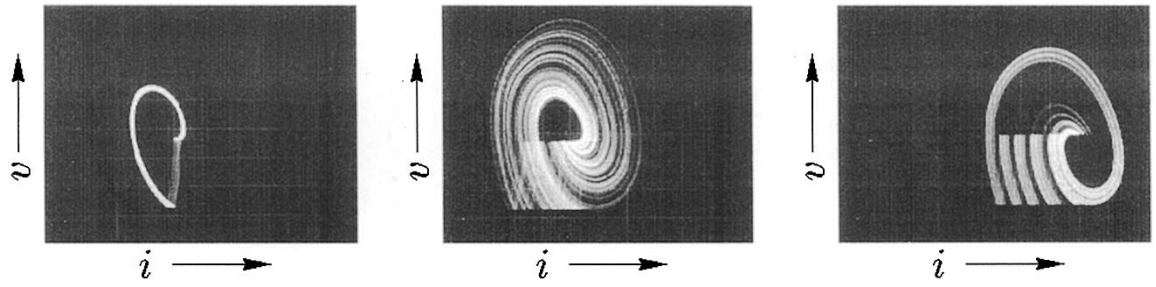

(a) (b) (c)

Fig. 15. Laboratory experiments-2. Chaotic attractors ($E_2 = 5.19\,\mathrm{V}$). (a) $E_1 = 2.04\,\mathrm{V}$. (b) $E_1 = 1.82\,\mathrm{V}$. (c) $E_1 = -10.21\,\mathrm{V}$. (v: 1.0 V/div, i: 2.1 mA/div).

putting

$$r_1 = \frac{1}{R_0 + R_1}, \qquad r_2 = \frac{1}{R_0 + R_2}, \qquad k = r\sqrt{\frac{C}{L}}$$
$$g_1 = 1 - (a_1 - r_1)\sqrt{\frac{L}{C}}, \qquad g_2 = 1 - (a_1 - r_2)\sqrt{\frac{L}{C}}$$
$$c_3 = \frac{3a_3}{C}\sqrt{\frac{L}{C}}, \qquad \hat{B}_1 = r_1\sqrt{L}E_1, \qquad \hat{B}_2 = r_2\sqrt{L}E_2 \tag{42}$$

and relabeling t' as t, we have the normalized equations (26) and (27), respectively, where

$$\hat{x} = \alpha x, \quad \hat{y} = \alpha y, \quad \alpha = \sqrt{\frac{1}{c_3}}, \quad \hat{B}_1 = \alpha B_1, \quad \hat{B}_2 = \alpha B_2. \tag{43}$$

When we fix the following parameters

$$L = 50\,\mathrm{mH}, \quad C = 0.1\,\mu\mathrm{F}, \quad R_0 = 0\,\Omega, \quad R_1 = 987\,\Omega$$
$$R_2 = 281\,\Omega, \quad r = 70.7\,\Omega, \quad h = -2.61\,\mathrm{V}$$
$$b = -0.26\,\mathrm{V}, \quad a_1 = 2.145 \times 10^{-3}, \quad a_3 = 6.9 \times 10^{-5} \tag{44}$$

these values correspond to the parameters shown in (36). Some typical periodic and chaotic orbits shown in Figs. 4 and 5 are also confirmed in laboratory experiments. Figs. 14 and 15 are obtained with various voltage values of E_1 according to the parameters of B_1 in Figs. 4 and 5.

IV. Concluding Remarks

We propose an efficient analyzing method for dynamical systems described by piecewise-defined functions. Local sections are defined at every break point and the Poincaré mapping is constructed as a composite map of the local mappings. As an illustrated example, we investigated the behavior of a Rayleigh-type oscillator with a state-dependent switch, and analyzed its bifurcation in detail. By varying the amplitude of an input voltage, we found many subharmonic bifurcation sets in the parameter plane. We also proposed to calculate the global bifurcation parameter values. Some theoretical results were confirmed by laboratory measurements.

A system which has m switches controlled by state-dependent switches can be analyzed in a similar way; however, calculation of the Jacobian matrix (21) becomes complicated in a high-dimensional system. Easy estimation of the Jacobian matrix is a future problem.

Acknowledgment

The authors would like to thank Prof. T. Saito, Dr. Y. Nishio, and Dr. T. Yoshinaga for their valuable comments and discussions on the basic matters of this work.

References

[1] R. W. Newcomb and N. El-Leithy, "Binary hysteresis chaos generator," in *Proc. IEEE/ISCAS*, Montreal, Canada, May 1984, pp. 856–859.
[2] T. Saito and S. Nakagawa, "Chaos from a hysteresis and switched circuit," *Philos. Trans. R. Soc. Lon.*, vol. A353, pp. 47–57, Nov. 1995.
[3] N. Inaba, T. Saito, and S Mori, "Chaotic phenomena in a circuit with a negative resistance and an ideal switch of diodes," *Trans. IEICE*, vol. E70, pp. 744–754, Aug. 1987.

[4] H. Kawakami and R. Lozi, "Switched dynamical systems—Dynamical of a class of circuits with switch—Structure and bifurcations of dynamical systems," in *Proc. RIMS Conf.*, S. Ushiki, Ed. Singapore: World Scientific, 1992, pp. 39–58.
[5] L. O. Chua, M. Komuro, and T. Matsumoto, "The double scroll family," *IEEE Trans. Circuits Syst.*, vol. CAS-33, pp. 1072–1118, Nov. 1986.
[6] W. C. Y. Chan and C. K. Tsu. "Bifurcations in current-programmed DC/DC boost converters," *IEEE Trans. Circuits Syst. I*, vol. 44, pp. 1129–1142, Dec. 1997.
[7] J. H. B. Deane, "Chaos in a current-mode controlled boost DC/DC converter," *IEEE Trans. Circuits Syst. I*, vol. 39, pp. 680–683, Aug. 1992.
[8] D. Hansel, G. Mato, and C. Meunier, "Clustering and slow switching in globally coupled phase oscillators," *Phys. Rev.*, vol. E48, pp. 3470–3477, 1993.
[9] S. G. Lee, S. Kim, and H. Kook, "Synchrony and clustering in two and three synaptically coupled Hodgkin-Huxley neurons with a time delay," *Int. J. Bifurcation and Chaos*, vol. 7, no. 4, pp. 889–895, 1997.
[10] Y. A. Kuznetsov, *Elements of Applied Bifurcation Theory*. Berlin, Germany: Springer-Verlag, 1996.

Takuji Kousaka (M'99) received the B.E., M.E., and D.E. degrees from Tokushima University, Tokushima, Japan, in 1994, 1996, 1999, respectively.

He is currently with Department of Electrical and Electronic Engineering, Fukuyama University, Fukuyama, Japan. His research interests are in bifurcations of discontinuous nonlinear differential equations and their control.

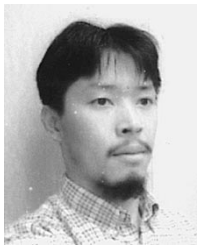

Tetsushi Ueta (M'94) received the B.E., M.E., and D.E. degrees from Tokushima University, Tokushima, Japan, in 1990, 1992, and 1996, respectively.

Since 1992, he has been with the Department of Information Science and Intelligent Systems, Tokushima University. From 1998 to 1999, he was a visiting scholar at the Department of Electrical and Computer Engineering, University of Houston, Houston, TX. His research interests include bifurcation problems of dynamical systems and their visualization.

Hiroshi Kawakami (M'81) received the B.E. degree from Tokushima University, Tokushima, Japan, in 1964, and the M.E. and D.E. degrees from Kyoto University, Kyoto, Japan, in 1966 and 1974, respectively, all in electrical engineering.

He is currently a Professor of Electrical and Electronic Engineering, Tokushima University, Tokushima, Japan. His research interest is in qualitative properties of nonlinear circuits.